

AD-A084 436

SRI INTERNATIONAL MENLO PARK CA
X-RAY PRODUCTION IN DEFENSE PLASMA FOCUS.(U)
MAR 80 D C GATES

F/G 20/8

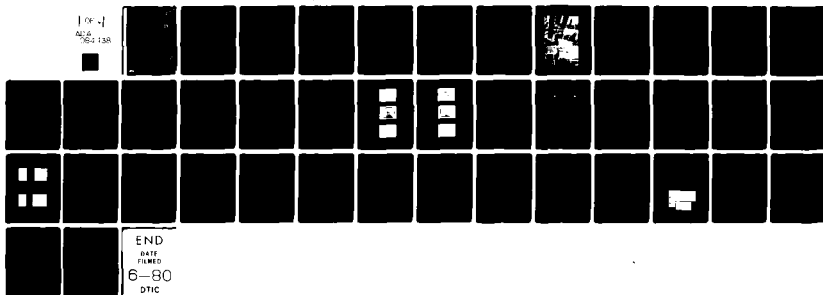
F44620-76-C-0034

UNCLASSIFIED

AFOSR -TR-80-0412

NL

1 of 4
ADA
764 138



END
DATE
FILMED
6-80
DTIC

ADA084438

18
19
AFOSR-TR-80-0412

11

6 X-RAY PRODUCTION
IN DENSE PLASMA FOCUS.

LEVEL II

9 Final Report. 1 Oct 75 - 30 Sep 79.

11 March 1980

10
By Duane C. Gates Senior Physicist
Engineering Sciences Laboratory

12 42

Prepared for:

U.S. Air Force
Office of Scientific Research
Bolling Air Force Base
Washington, D.C. 20332

Contract F44620-76-C-0034

15

SRI Project 4640

16 2341

17 11

DTIC
ELECTE
S MAY 20 1980 D
D

Approved for public release:
distribution unlimited.

use ->

SRI International
333 Ravenswood Avenue
Menlo Park, California 94025
(415) 326-6200
Cable: SRI INTL MPK
TWX: 910-373-1246

410281

80 5 14

084



Unclassified

SECURITY CLASSIFICATION OF THIS PAGE (When Data Entered)

REPORT DOCUMENTATION PAGE		READ INSTRUCTIONS BEFORE COMPLETING FORM	
1. REPORT NUMBER AFOSR-TR- 80-0412		2. GOVT ACCESSION NO.	
4. TITLE (and Subtitle) X-RAY PRODUCTION IN DENSE PLASMA FOCUS		3. RECIPIENT'S CATALOG NUMBER	
7. AUTHOR(s) Duane C. Gates		5. TYPE OF REPORT & PERIOD COVERED Final Report 1 October 1975 to 30 September 1979	
9. PERFORMING ORGANIZATION NAME AND ADDRESS SRI International 333 Ravenswood Avenue Menlo Park, California 94025		6. PERFORMING ORG. REPORT NUMBER SRI Project 4640	
11. CONTROLLING OFFICE NAME AND ADDRESS Director of Physics, Attn: NP Air Force Office of Scientific Research Bolling AFB, Washington, D.C. 20332		8. CONTRACT OR GRANT NUMBER(s) F44620-76-C-0034 <i>new</i>	
14. MONITORING AGENCY NAME & ADDRESS (if diff. from Controlling Office)		10. PROGRAM ELEMENT, PROJECT, TASK AREA & WORK UNIT NUMBERS 61102F 2301/A7	
16. DISTRIBUTION STATEMENT (of this report) Approved for public release; distribution unlimited.		12. REPORT DATE March 1980	
		13. NO. OF PAGES 40	
		15. SECURITY CLASS. (of this report) Unclassified	
		15a. DECLASSIFICATION/DOWNGRADING SCHEDULE NA	
17. DISTRIBUTION STATEMENT (of the abstract entered in Block 20, if different from report)			
18. SUPPLEMENTARY NOTES			
19. KEY WORDS (Continue on reverse side if necessary and identify by block number) Plasma focus X-ray yield Puffed gas High-voltage			
20. ABSTRACT (Continue on reverse side if necessary and identify by block number) - This program investigated the operation of plasma focus (PF) devices at high voltage. Discharge formation, energy transfer, and X-ray emission were studied at 60 kV (108 kJ) with a 10X15-cm diameter PF gun. A model was developed that relates the optimum pressure for discharge formation to the electric field condition for maximum ionization efficiency. The energy transfer efficiency was measured and found to be in reasonable agreement with the theory of Bruzzone et al. A PF model is described that interprets the observed X-ray emission from argon in terms of both plasma processes and focus-produced electron beam phenomena: The model predicted that a neon plasma would radiate 1 percent of the stored energy. The construction of a 120-kV (108 kJ) plasma focus system is described.			

Unclassified

SECURITY CLASSIFICATION OF THIS PAGE (When Data Entered)

CONTENTS

LIST OF ILLUSTRATIONS	v
LIST OF TABLES	vii
I INTRODUCTION	1
II 60-kV PLASMA FOCUS SYSTEM	3
III GEOMETRY AND ELECTRODYNAMICS STUDIES	7
A. Geometry	7
B. Electrodynamics	8
1. Discharge Formation Model	8
2. Energy Transfer	12
IV X-RAY STUDIES	17
A. Puffed Gas System	17
B. Instrumentation and Measurements	19
C. Discussion of Results	24
D. Radiation Model Prediction for Neon	26
V 120-kV PLASMA FOCUS SYSTEM	31
VI RECOMMENDATIONS FOR FURTHER RESEARCH	35
VII LIST OF PUBLICATIONS RESULTING FROM THIS PROJECT	37
REFERENCES	39

Accession For	
NTIS GRA&I	<input checked="" type="checkbox"/>
DDC TAB	<input type="checkbox"/>
Unannounced	<input type="checkbox"/>
Justification	
By _____	
Distribution/	
Availability Codes	
Dist.	Avail and/or special
A	

1. SOURCE: AFOSR/XXX, AFOSR/XXX (AFSC)
 2. DATE: 1980-12-12
 3. TITLE: [REDACTED]
 4. SUMMARY: [REDACTED]
 5. RESEARCH AND DEVELOPMENT AND IS
 6. COVERED BY AFOSR/XXX (AFSC) 100-12 (7b).
 Distribution is unlimited.
 A. D. BLOSE
 Technical Information Officer

ILLUSTRATIONS

1	Dense Plasma Focus System, Showing Right Half of Capacitor Bank, Current Collector Ring, and Switch Pressurization System	4
2	DPF System	5
3	DPF Control System	6
4	Model 10X15-3 Plasma Focus Geometry	9
5	Insulator Coverage For Discharge Initiation	11
6	Energy Transfer Diagnostics Schematic	13
7	Model 10X15-3 Plasma Focus Operated at 60 kV and 6 Torr--H ₂	15
8	Model 10X15-3 Plasma Focus Operated at 60 kV and 6 Torr--H ₂ with Pulsed Argon	16
9	Puffed Gas Valve for Plasma Focus	18
10	Light-Sensing Trigger and Pulsed Power Circuit for Puffed Gas System	18
11	Spira-Lite Trigger Circuit for Puffed Gas System	19
12	Filtered Fluorescer PIN X-Ray Detector	21
13	Response Functions of Filter-Fluorescer X-Ray Detectors . . .	22
14	X-Ray Signals from PIN Detectors in Fluorescer and Filtered PIN Geometries	23
15	Power Radiated by Neon Plasma	30
16	Capacitor Bank and Master Switch Circuits for 120-kV System	32
17	120-kV, 54-kJ Section of Capacitor Bank for a Plasma Focus Device	33
18	Thin-Wall Cylinder and Magnified Wall Cross Section	35

PRECEDING PAGE BLANK-NOT FILLED

TABLES

1	Dimensions of Experimental Plasma Gun Components	7
2	Spectral Characteristics of Argon	20
3	Radiation Models for Argon	24
4	Spectral Characteristics of Neon	28

I INTRODUCTION

Since the discovery of the plasma focus (Mather, 1964),* the device has come under investigation in many laboratories. Much of the early work has been reviewed (Mather, 1971a; Decker, 1976). At the inception of this research program in 1975, most plasma focus (PF) devices were operated at voltages below 50 kV. However, the benefit of high voltage operation was recognized early as a means to obtain higher peak current per unit capacitor bank energy and to improve the radiation output efficiency of the plasma focus. More recent theoretical studies have reported and explained the observed power-law scaling relation for radiation output (Imshennik, 1973; Trunk, 1975; Kaeppler, 1977). Consequently, there has been a trend to build larger machines that operate at higher voltages (Mather, 1971b; Downing, 1973; Ware, 1973; Decker, 1977).

This report summarizes the studies undertaken at SRI International (SRI) to investigate X-ray production in high-voltage plasma focus devices, with emphasis on methods to increase the X-ray yield efficiency of PF systems. The scope of the work covered three general categories:

- Current sheet propagation and energy transferred into the plasma focus.
- Introduction of high-Z materials into the plasma focus.
- Heating the plasma focus.

The following sections describe the results of studies on discharge formation and energy transfer from the capacitor bank into the plasma gun and plasma focus. We also describe the results of the measurements on argon K-line radiation obtained by operating the system with puffed gas injection of argon and with argon-seeded hydrogen gas. This radiation is explained in terms of a combined plasma model and beam target model for radiation. Model predictions of higher X-ray yield from neon gas are described. We also describe the 120-kV capacitor bank that was built but not operated. In addition to summarizing results of this program that have been published (Gates 1977, 1978a, 1978b), we have included for completeness some additional illustrations of the apparatus and description of theoretical results.

*References are listed at the end of this report.

II 60-kV PLASMA FOCUS SYSTEM

Much of the apparatus used in this work was obtained from Los Alamos Scientific Laboratories (LASL); Dr. Kenneth Ware of LASL served as a consultant on details of assembling these components. Items added at SRI to achieve a working system included the high-voltage power supply, trigger circuits for the switches, a pressurization and purging system for the switches, electrodes, diagnostics, and a screen room.

The capacitor bank is a 60-kV, 60- μ F, 108-kJ system that delivers about 2.2 MA into a short circuit with a rise time of about 2.6 μ s. The external inductance is fairly large, about 44 nH. At 60 kV, the capacitor bank delivers about 1.5 MA into a plasma gun. A photograph of the capacitor bank and plasma focus system is shown in Figure 1. The modular configuration of the capacitor bank is shown schematically in Figure 2. Eight capacitors (C_i) are assembled into a common module with one spark-gap switch (S_i). The capacitors are charged and the switch is triggered by a pulse through the isolation transformer (T_i). Before triggering, the middle electrode of the spark gap is maintained at a voltage midway between the charging voltage and ground by the resistive divider network (R). The ground return during charging is through the inductor L. When the gap is triggered, the voltage is applied to the PF load, which then provides the discharge path for the module energy. Each module is connected to the load by 12 parallel coaxial cables.

The charging and triggering system for the four-module capacitor bank is shown in Figure 3. The master switch gap (S) is used to trigger the four spark gaps in the capacitor bank. The master gap is a pressurized spark gap on a single 60-kV capacitor. This switch is triggered by a pulse from a trigger generator, which also accepts a prefire pulse back from the PF gun. If one of the bank spark gaps prefires before the master gap fires, the prefire pulse triggers all the bank spark gaps within a short time: this feature prevents damage to the system. One dump resistor, R_i , is provided for each module. These resistors and the relay connections to ground constitute the capacitor bank dump circuit. When the capacitor bank is charged, it can be either triggered or dumped from the control console.

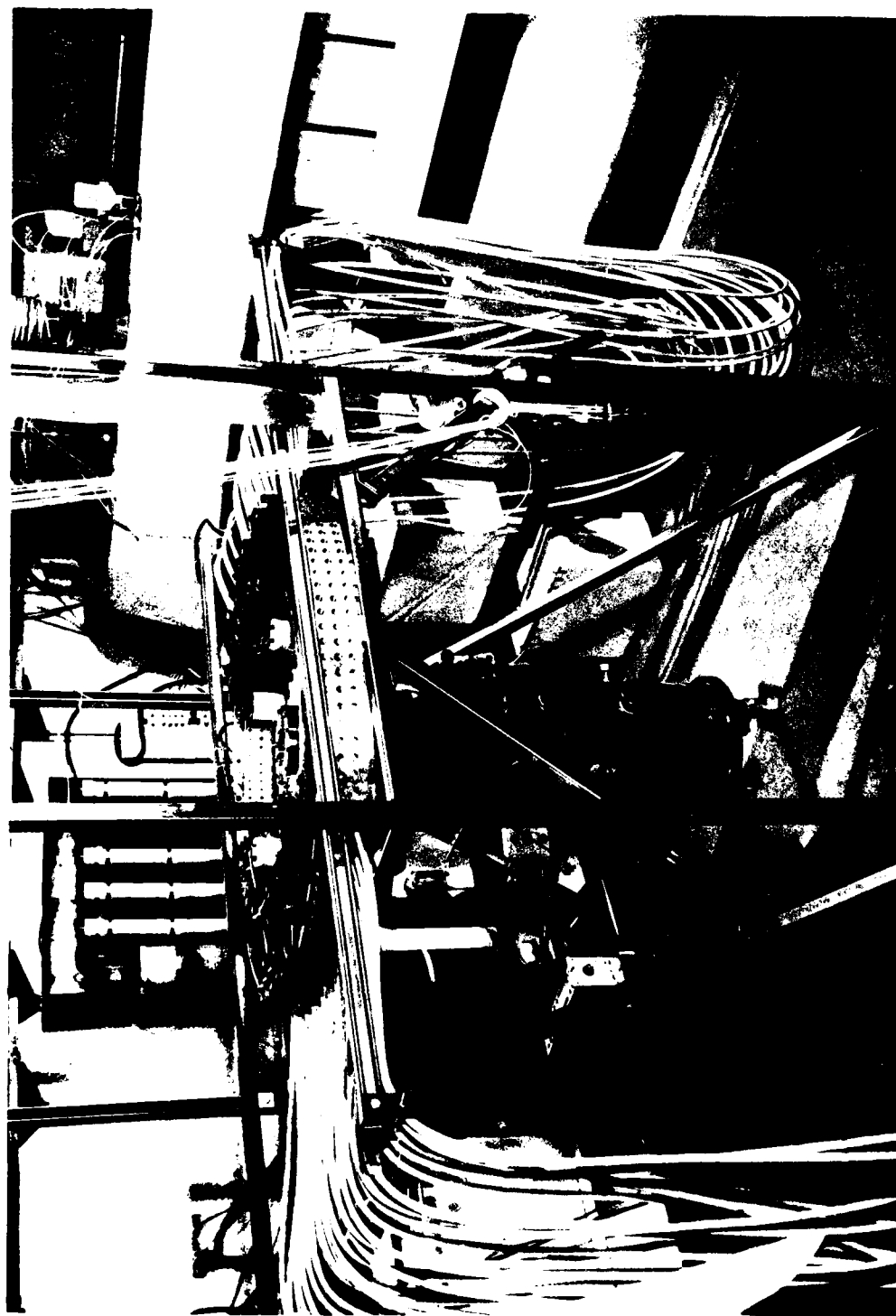
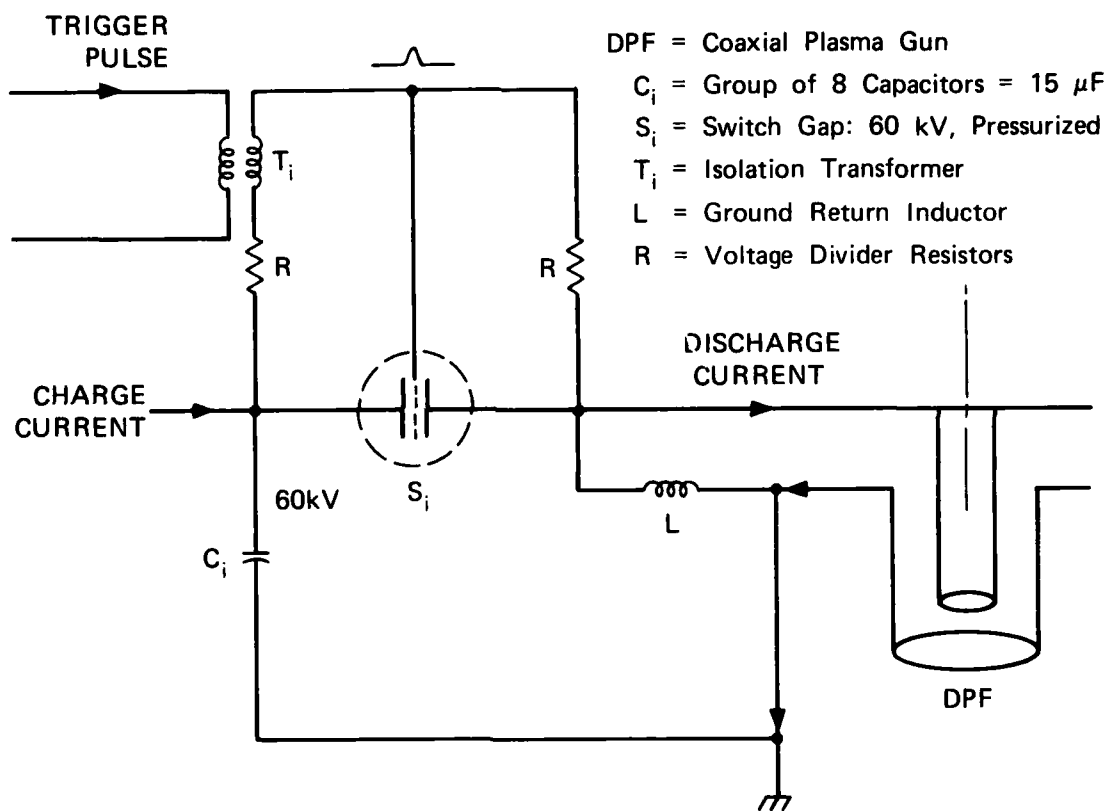
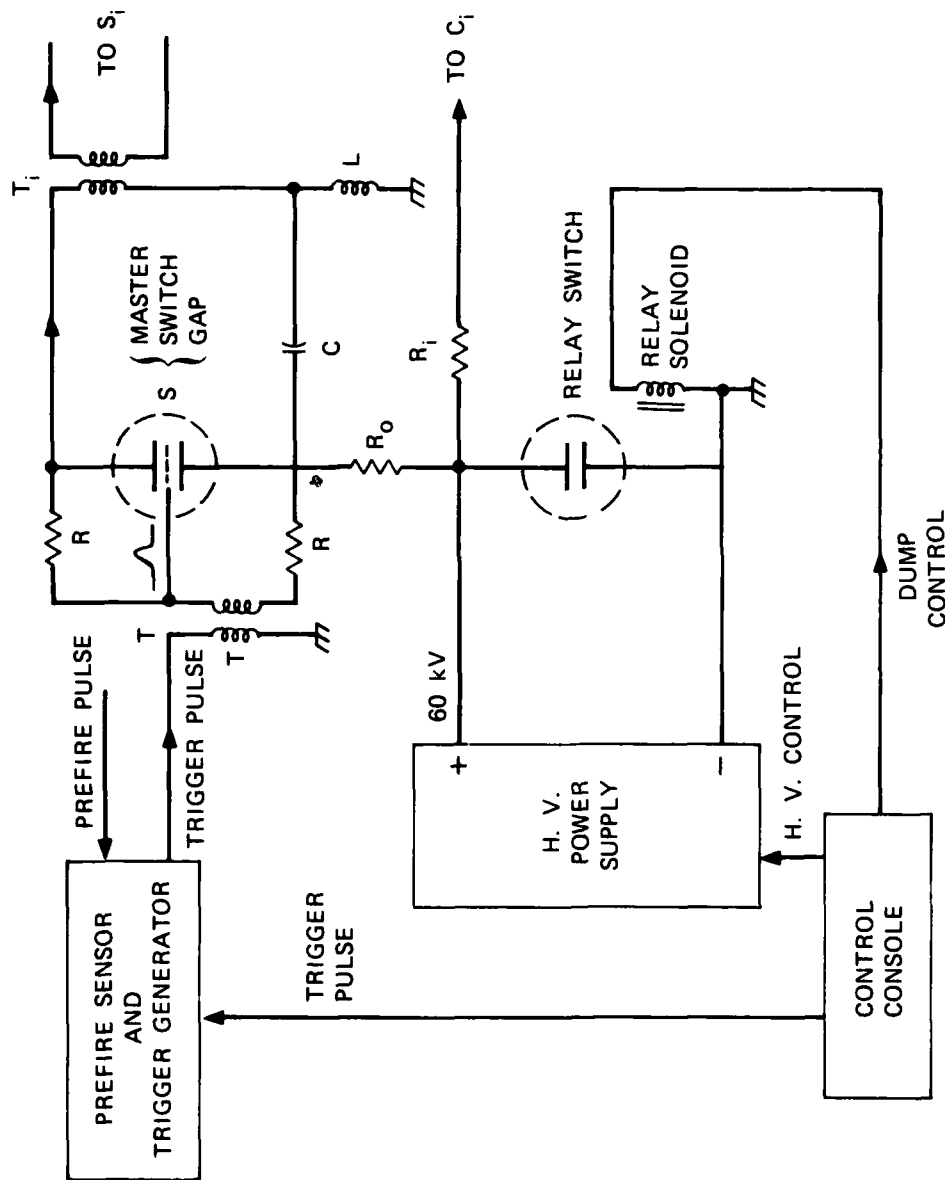


FIGURE 1 DENSE PLASMA FOCUS SYSTEM, SHOWING RIGHT HALF OF CAPACITOR BANK, CURRENT COLLECTOR RING, AND SWITCH PRESSURIZATION SYSTEM (ON WALL)



MA-319583-68

FIGURE 2 DPF SYSTEM



MA-319583-67

FIGURE 3 DPF CONTROL SYSTEM

Functions: Charge Capacitor Bank;
Dump Bank Energy (Safety);
Trigger Bank Switch Gaps to Drive DPF.

III GEOMETRY AND ELECTRODYNAMICS STUDIES

A. Geometry

The PF system was operated with the five plasma gun geometries whose electrode and insulator dimensions are given in Table 1. Each of the plasma guns had a 10-cm diameter center electrode (CE) and a 15-cm long insulator: they differed principally in the CE length and in the type of outerelectrode (OE)--planar or barred. Most of the studies were done with either the model 10X35-2 or model 10X15-3 devices. The performance of these units is described briefly in the following paragraphs.

Table 1

DIMENSIONS OF EXPERIMENTAL PLASMA GUN COMPONENTS*

Component	Model				
	10X35-1	10X35-2	10X15-1	10X15-2	10X15-3
Anode (CE)					
Diameter (OD)	10 [†]	10 [†]	10 [†]	10 [†]	10
Length beyond insulator	41.8	13.5	41.8	13.5	25.2
Tip shape	Rounded	Hollow	Rounded	Hollow	Hollow
Bore (ID)	1.3	7.6	1.3	7.6	7.6
Cathode (OE)					
Diameter (ID)	35	35	15	15	15
Length	106.2	106.2	66.5	66.5	66.5
Rods (No. × dia.)	Solid	Solid	24X1.3	24X1.3	24X1.3
Insulator					
Length (exposed)	15.3	15.3	15.3	15.3	15.3
Diameter (OD)	11.3	11.3	11.3	11.3	11.3
Wall thickness	0.6	0.6	0.6	0.6	0.6

* All dimensions in centimeters.

[†]Reduced to 7.6 cm beneath insulator (undercut length = 16 cm).

Much of the X-ray diagnostic and the puffed-gas operation was done with the 10X35-2 plasma gun geometry. The anode was a 10-cm-diameter hollow CE; the pyrex insulator about 15-cm long and the center electrode extended 13.5 cm beyond the insulator. No outer electrode was used, hence the plasma gun had a planar cathode extending to the 35-cm diameter of the vacuum chamber wall. (Thus it was in essence a 35-cm by 10-cm gun.)

We made no attempt to optimize the 10X35-2 electrode geometry for best focusing; our intention was rather to remove any obstacle to the current sheet symmetry for the high voltage studies. (With this geometry, the focus occurs before the current sheet hits the vacuum chamber wall.)

The optimum hydrogen fill pressures for this system were determined by experiment to be 3.2 torr at 40 kV, 4 torr at 45 kV, and 5 torr at 50 kV. The average current sheet speed from the insulator to the end of the CE was 6 cm/ μ s; the time integral of voltage divided by the current yields an estimate of the internal inductance history. At pinch time, the internal inductance was about 80 nH, most of which was generated before the pinch collapse. The current sheet must be nearly out to the vacuum wall to account for this much inductance. (This conclusion is also consistent with the observed sheet speed.) We observed that when the mass loading was held at a given value, the sheet current and time of focus remain constant within ± 5 percent regardless of the operating mode (i.e., pure hydrogen, hydrogen + pulsed argon, or hydrogen + static argon).

From our studies of plasma gun electrodynamics at lower voltages, we designed the model 10X15-3 plasma gun, which operated successfully at 60 kV. The best pressure for pinching at peak current was 7 torr. This geometry was designed for improved operation above 45 kV where erratic focusing had been observed with previous geometries. The CE design used in the other plasma gun included an undercut beneath the insulator (1/2 inch on radius) to increase the electric field there during discharge initiation: This undercut was eliminated in the 10X15-3 design to produce a lower electric field across the insulator when operating at 60 kV.

A schematic drawing of the plasma gun is shown in Figure 4: the model illustrated is 10X15-3, which uses a barred cathode. (The dimensions are given in Table 1.) Figure 4 also shows a pulsed valve and tube for injecting gas at the focus; this apparatus is described in Section IV-A.

B. Electrodynamics

1. Discharge Formation Model

Proper discharge initiation--the first 100 ns or less--is very important for current sheet symmetry and efficiencies of the snow-plow

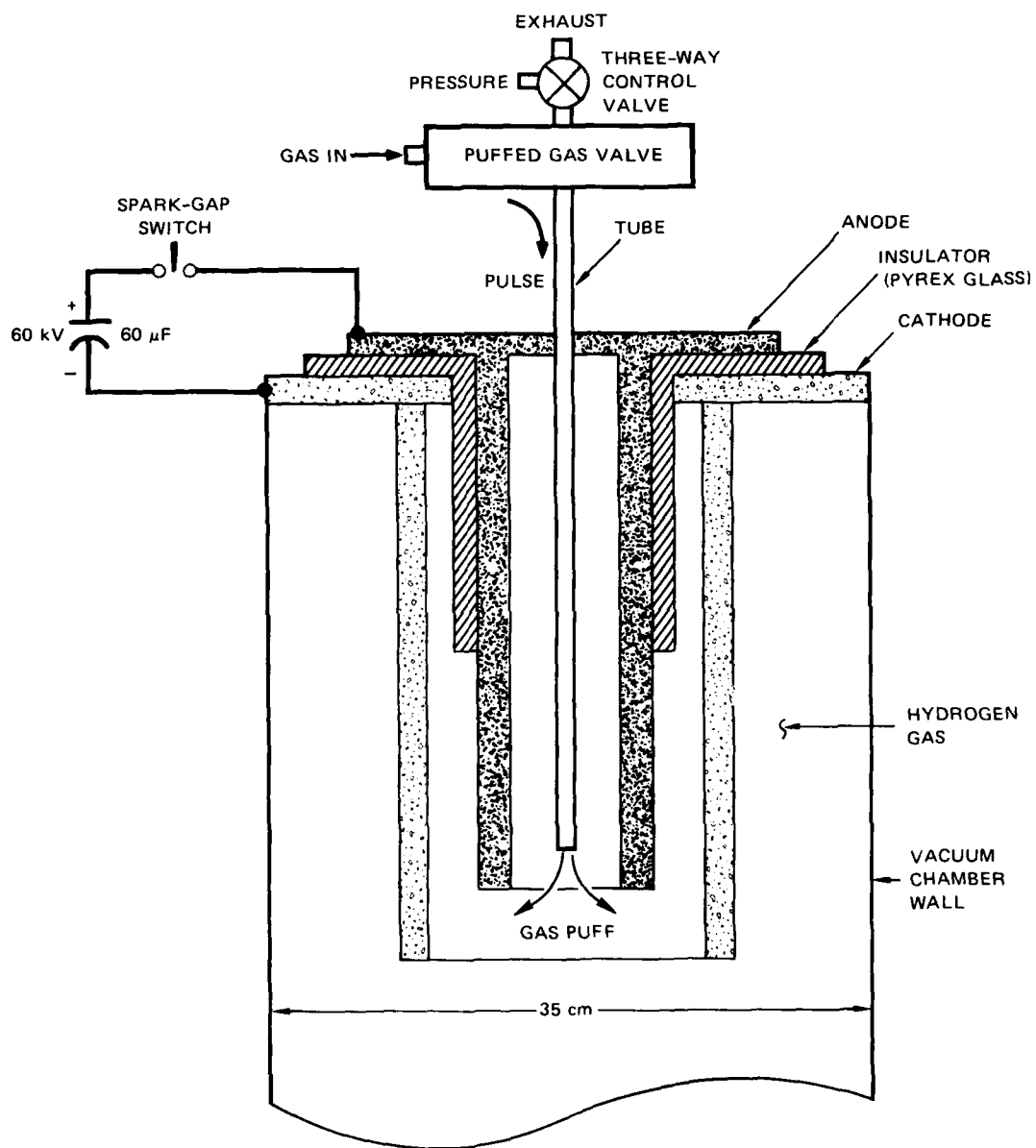


FIGURE 4 MODEL 10X15-3 PLASMA FOCUS GEOMETRY

operation. The following model of discharge formation is useful in designing the breech area of plasma guns and may be used to estimate the proper operating pressure for given initial electric field conditions.

The model assumes that for a rapid breakdown and complete ionization, the following conditions for discharge formation must be fulfilled:

- High ionization rate
- Insulator coverage.

For avalanche electrons, the ionization efficiency, ϵ , is defined as (ionization pairs formed)/(energy gain in E-field). Choosing the electric field and pressure at the insulator to provide a maximum ionization efficiency provides the highest ionization rate. For hydrogen, the relation between the electric field and pressure for maximum ionization efficiency is given by (Brown, 1959):

$$E(\epsilon_{\max}) = 1.4 \times 10^4 p(\text{torr}) \quad . \quad (\text{volt/meter}).$$

The electric field at the insulator is given by

$$E = V_i/d = V_o L'_i/L_x + dL'_i) \quad ,$$

where

V_i = voltage drop across the insulator

L_x = external inductance

L'_i = inductance per unit length of the insulator

d = insulator length

V_o = initial bank voltage.

These two equations may be combined to find the optimum pressure for maximum ionization efficiency, given by

$$p \left[\epsilon_{\max}^{(H_2)} \right] = \frac{L'_i}{L_x + dL'_i} \cdot \frac{V_o}{14 \times 10^3} \quad . \quad (\text{torr}).$$

For the SRI Model 10X15-3 gun, the optimum pressure in hydrogen is about 2.4 torr.

The maximum ionization efficiency in argon occurs near the same value of E/p as in hydrogen. As a result, the optimum pressure in argon is about 0.7 that in hydrogen. However, proper mass loading for operation with argon requires a much lower pressure--far from the optimum value. It is therefore quite reasonable to pulse in the argon at the focus region, where it will not perturb the initial discharge conditions.

Our meaning of the second condition for proper discharge initiation, insulator coverage, is illustrated by Figure 5. A sheath is formed at the cathode after the initial gas breakdown. The conditions at this time are somewhat similar to an abnormal glow discharge, but with time dependence. The sheath is thin compared to the length of the insulator, and most of the insulator voltage drop appears across it. Electrons are released from the cathode by ion bombardment and by photons from the gas.

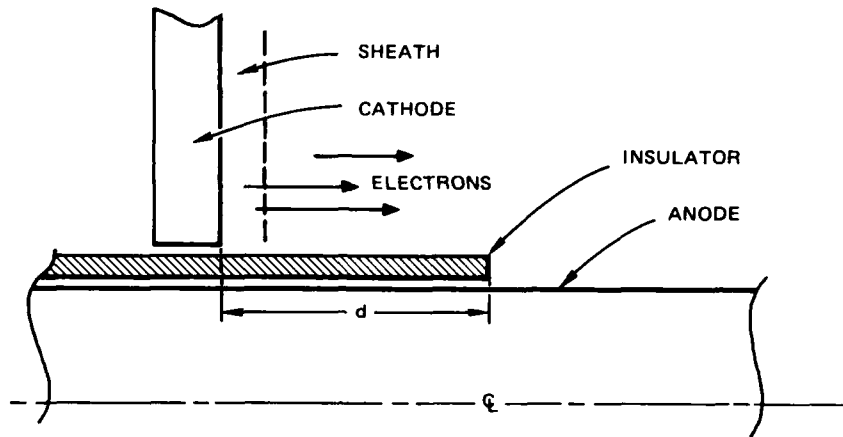


FIGURE 5 INSULATOR COVERAGE FOR DISCHARGE INITIATION

These electrons are accelerated across the sheath and give up their kinetic energy to ionizing collisions in the gas. To provide for rapid and continuing ionization across the whole length of the insulator, we require that the range of these electrons be greater than (or approximately equal to) the insulator length:

$$\text{Condition: } R_e \geq d$$

The range of electrons, R_e , may be expressed approximately as (Brown, 1959)

$$R_e \approx 3 \times 10^{-4} V_c / p \quad , \quad (\text{meters})$$

where V_c is the cathode voltage drop;

$$V_c = V_i = Ed \quad .$$

These two equations give

$$R_e \approx 3 \times 10^{-4} (E/p)d \quad .$$

Applying our condition for insulator coverage, we obtain

$$p \leq 3 \times 10^{-4} E \quad .$$

In terms of the pressure for maximum ionization rate in hydrogen, we then obtain an upper limit on operating pressure given by

$$p \lesssim 4p \left[\epsilon_{\max} (H_2) \right] \quad .$$

The last relationship means that the electrons emitted from the cathode still traverse the insulator length if the hydrogen pressure is less than four times the optimum pressure. At greater pressures, a positive column must be formed in the remaining distance to the anode. We expect that the presence of a positive column (with its lower ionization and conductivity) would tend to increase the possibility of current sheet asymmetries, instabilities, and porosity.

2. Energy Transfer

After the current sheet is formed, its propagation is governed by the balance of magnetic pressure and momentum given by $B^2/2\mu_0 = \rho_0 v^2$. Bruzzone et al. developed a model that includes inertia of the current sheet mass (Bruzzone, 1976). They applied their model to plasma focus devices used at a number of laboratories to estimate the energy transfer to the plasma. They showed that there is an apparent correlation of energy transfer to the plasma with the neutron yield of the devices. It seems reasonable, therefore, to look for a similar correlation with X-ray yield to determine if the energy transfer to the plasma affects the X-ray output.

The energy transfer to a plasma focus device can be expressed as

energy delivered = work on plasma + magnetic energy, or

$$\int VI dt = W_p + LI^2/2 \quad ,$$

where

VI = power delivered

W_p = work on plasma

$LI^2/2$ = stored magnetic energy.

The efficiency, ϵ_p , of energy transferred to the plasma is defined as

$$\epsilon_p = W_p / (CV_o^2/2)$$

These quantities can be obtained using an X-Y display oscilloscope, where

$$x = \int V dt, \quad y = \int I dt$$

By integrating the signals from voltage and dI/dt probes and displaying them on an X-Y oscilloscope, we obtain the following relationships:

$$\int V I dt = \int y dx \text{ (area under the curve)}$$

$$LI^2/2 = yx/2$$

$$W_p(\text{rundown}) = \int_0^1 y dx - y_1 x_1 / 2$$

$$W_p(\text{pinch}) = \int_1^2 y dx - (y_2 x_2 - y_1 x_1) / 2$$

Interpretation of the oscillograph is illustrated in Figure 6, where W_p for the rundown and the pinch phases of the discharge are indicated as areas under the curve.

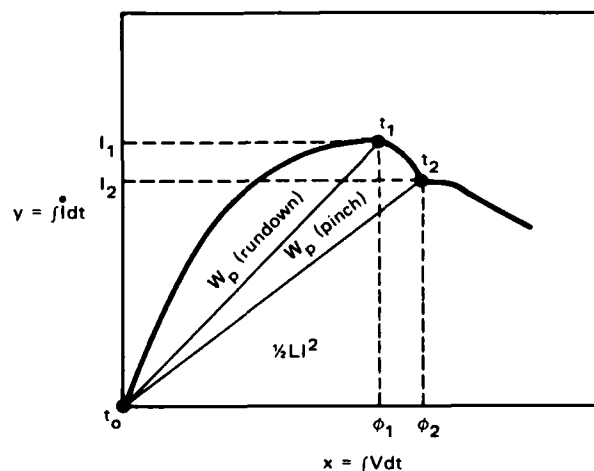


FIGURE 6 ENERGY TRANSFER DIAGNOSTICS SCHEMATIC

Examples of energy-transfer measurements are shown in Figures 7 and 8. In Figure 7, the plasma focus was operated at 60 kV with 6 torr of pure hydrogen and no argon. Several features may be noted here: relatively small energy transfer to the pinch, short X-ray pulse, and narrow voltage and dI/dt pulses at pinch time. Figure 8 is an example at 60 kV with argon pulsed in to a static fill of hydrogen. Here we note a relatively large energy transfer, long X-ray pulse with an additional very narrow X-ray spike super-imposed, and relatively wide voltage and dI/dt pulses at pinch time.

We obtained the following energy-transfer results:

$$\epsilon_p(\text{rundown}) \approx 19 \text{ percent}$$

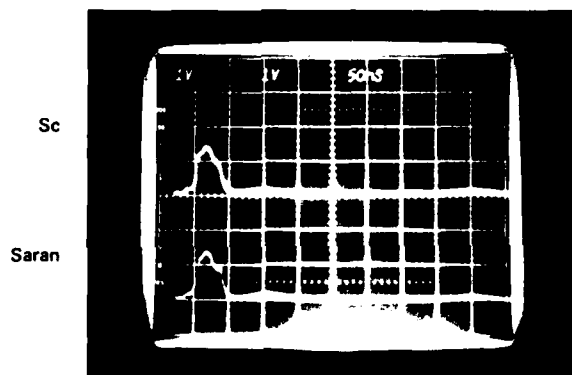
$$\epsilon_p(\text{pinch}) \approx 12 \text{ to } 24 \text{ percent (shot-to-shot variation)} \quad .$$

The gun parameters were put into Bruzzone's model, which predicted an energy transfer efficiency of about 15 percent. The Bruzzone model assumed a snowplow mass collection of 30 percent. The difference between the measured and predicted values could be explained by a larger mass collection efficiency for the Model 10X15-3 device. As for correlation of energy transfer with the X-rays, we note that there was no apparent correlation of energy transfer with the very narrow X-ray spike (about 10-ns duration); this spike is probably associated with a beam-formation phenomenon in the focus. The efficiency during the rundown phase was fairly consistent from shot to shot, whereas the narrow X-ray spike was not always present. The long duration component of the X-ray pulse, present on every shot, is probably associated with plasma phenomena. There may be a correlation with the pinch energy transfer and the amount of X-ray radiation from the long-duration components of the X-ray pulse; however, more data are needed to make a definitive determination. In addition, the plasma focus conditions have not yet been optimized at 60 kV. Therefore, it may be possible to obtain narrower pulses than we observed so far with pulsed argon.



Time — 1 μ s/division →

(a) VOLTAGE AND di/dt



Time — 50 ns/division →

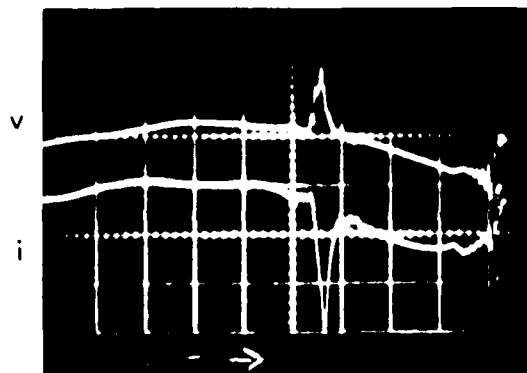
(b) PIN X-RAY DETECTORS FILTERED BY Sc AND SARAN (ROSS PAIR)



$x = \int V dt$

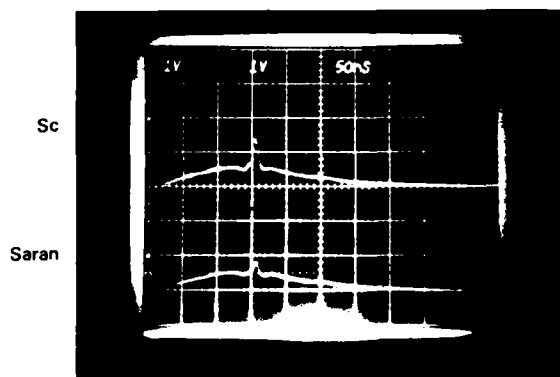
(c) ENERGY TRANSFER

FIGURE 7 MODEL 10X15-3 PLASMA FOCUS OPERATED AT 60 kV AND 6 TORR — H_2



Time — 1 μ s/division →

(a) VOLTAGE AND di/dt



Time — 50 ns/division →

(b) PIN X-RAY DETECTORS FILTERED BY Sc AND SARAN (ROSS PAIR)



$x = \int V dt$

(c) ENERGY TRANSFER

FIGURE 8 MODEL 10X15-3 PLASMA FOCUS OPERATED AT 60 kV AND 6 TORR — H_2 WITH PULSED ARGON

IV X-RAY STUDIES

A. Puffed Gas System

Puffed gas was used primarily to separate the conditions at the focus and the breech: With the plasma gun, the ideal conditions for a discharge initiation and propagation of the current sheet in the axial direction are not necessarily the same conditions desired for focusing. Past experience with argon demonstrated that the current sheet propagation was poor when argon was used in the device. By puffing in argon, we could initiate the discharge in substantially pure gas and then focus on argon. Puffing in the argon allowed us to pinch on a higher argon concentration than would be possible with a static mixture of argon and hydrogen.

The puffed gas valve was mounted on the high voltage side of the system, as shown in Figure 4. The gas was brought to the focus through a long 3-mm-ID tube on the axis. The end of the tube was located 2-cm inside the center electrode. Argon gas was usually puffed into a static hydrogen fill at a pressure that was appropriate for pinching near peak current.

Figure 9 is a schematic diagram of the valve, which contains a small gas reservoir that is isolated from the inlet tube by a mylar diaphragm that seals against an o-ring. This seal is maintained by gas pressure on the other side of the diaphragm. A solenoid valve releases the confining pressure to introduce a puff of gas into the inlet tube to the focus. Typically about $100 \text{ cm}^3\text{-atm}$ of argon is puffed in, which eventually increases the chamber static pressure by 0.8 torr.

Since the valve is mounted on the high voltage side of the system, it is powered by a remote control power supply that is initiated with a strobed light: This circuitry is shown in Figure 10. A photosensor permits the valve to be triggered by a flash of light from a Spira-Lite flash lamp and control circuit that is located at ground potential. The circuit diagram for triggering the flash lamp is shown in Figure 11.

The puffed gas valve operated fairly slowly. A hot wire filament was used to measure the time of arrival of the puff at the plasma focus and the rise time to peak pressure. The pressure began to rise about 10 ms after the solenoid was energized and reached a peak pressure about 20 ms thereafter. Because we always operated with a static filling of hydrogen into which the gas was puffed, the slow rise time did not seem to prevent separation of the gas species at the focus from those at the breech of the plasma gun.

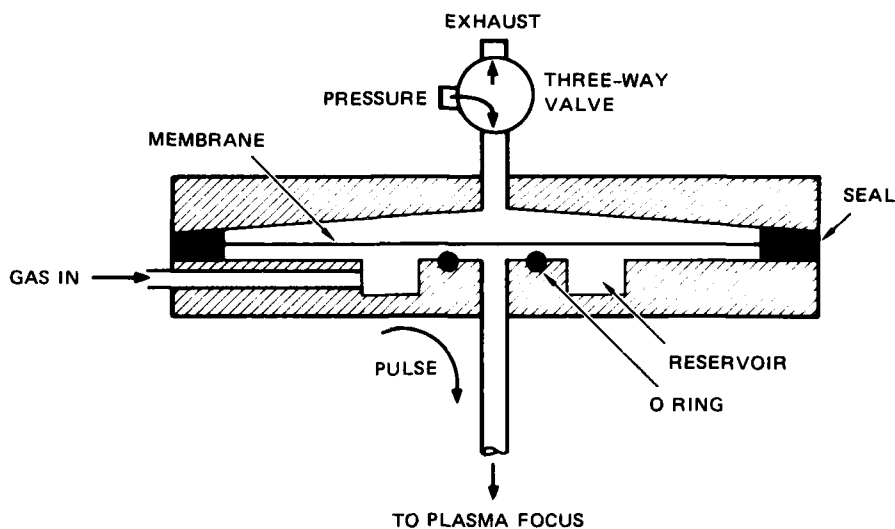


FIGURE 9 PUFFED GAS VALVE FOR PLASMA FOCUS

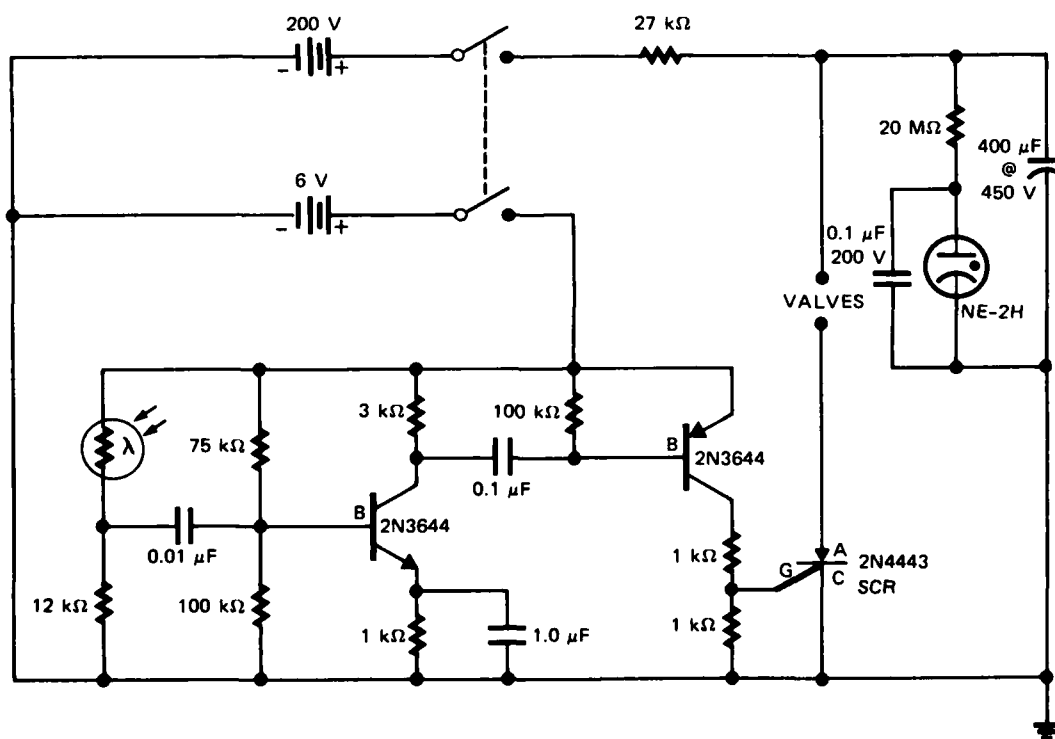


FIGURE 10 LIGHT-SENSING TRIGGER AND PULSED POWER CIRCUIT FOR PUFFED GAS SYSTEM

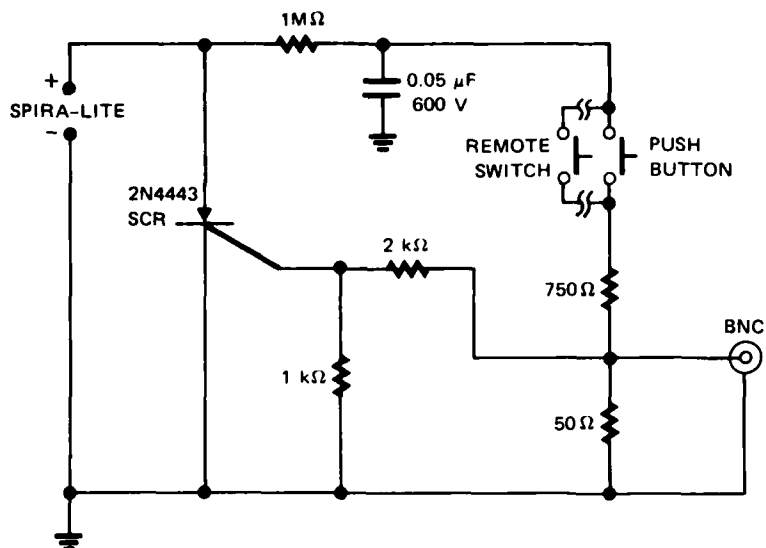


FIGURE 11 SPIRA-LITE TRIGGER CIRCUIT FOR PUFFED GAS SYSTEM

B. Instrumentation and Measurements

The spectral characteristics of argon are shown in Table 2. The argon K-edge is at 3.2 keV. Table 2 shows that all of the lines from 2p to 1s transitions of any charge state have energies near 3 keV. For this reason, an X-ray detector energy band of 2.8 to 4.5 keV was used for discriminating line radiation. Highly ionized argon species also produce a recombination continuum that starts at a threshold energy determined by the ionization potential of the recombined ion. These lower-bound energies are also shown in Table 2: the recombination into hydrogen-like or helium-like ions produces a spectrum that mostly lies outside of the energy band used to detect the line radiation.

X-ray measurements were made using lithium-drifted silicon PIN detectors. Two detector geometries were used: fluorescer type and filter type. In the fluorescer geometry, the detector is outside of the direct line of the X-rays from the focus and views a fluorescer with a filter between it and the focus. In the filter geometry, the detector is in a direct line to the source with an appropriate K-edge filter in front.

Table 2
SPECTRAL CHARACTERISTICS OF ARGON

Lines		Lower Bound of Recombination Spectrum	
Charge State	$E_v(2p - 1s)$ (keV)	Ion Specie	$E_v(\min)$ (keV)
0	3.0	18+ \rightarrow 17+	4.4
15+	3.1	17+ \rightarrow 16+	4.1
16+	3.1	16+ \rightarrow 15+	0.9
17+	3.3		

The fluorescer geometry is shown in Figure 12. The combination of filter and fluorescer and detector as shown in this figure provides an energy band within which the detector has its greatest sensitivity. Chlorine, scandium, iron, and zinc are used to provide energy bands of 2.8 to 4.5 keV, 4.5 to 7.1 keV, and 7.1 to 9.7 keV. The X-ray detector energy-response functions of these three detector channels are shown in Figure 13. (The attenuation resulting from the beryllium window is not included in these curves.)

The advantage of the fluorescer geometry is that only one detector is needed to provide a response in a given energy band. However, as can be seen in Figure 13, there is some undesirable out-of-band response. Note in this figure that the three channels differentiate between the lines from argon, iron, and copper. This type of detector channel also has a very low sensitivity.

An oscillograph of the detector signals from the two lower-energy channels is shown in Figure 14(a). Note the very narrow pulse width associated with the beam phenomenon. The X-ray output is most intense in the 2.8- to 4.5-keV band, indicating strong line emission from argon.

The filtered detector geometry makes use of two PIN detectors, each with different K-edge filters in front, to form a Ross filter pair. The difference in signal between the two detectors represents the energy in the band between the K-edges of the filters. The same three energy

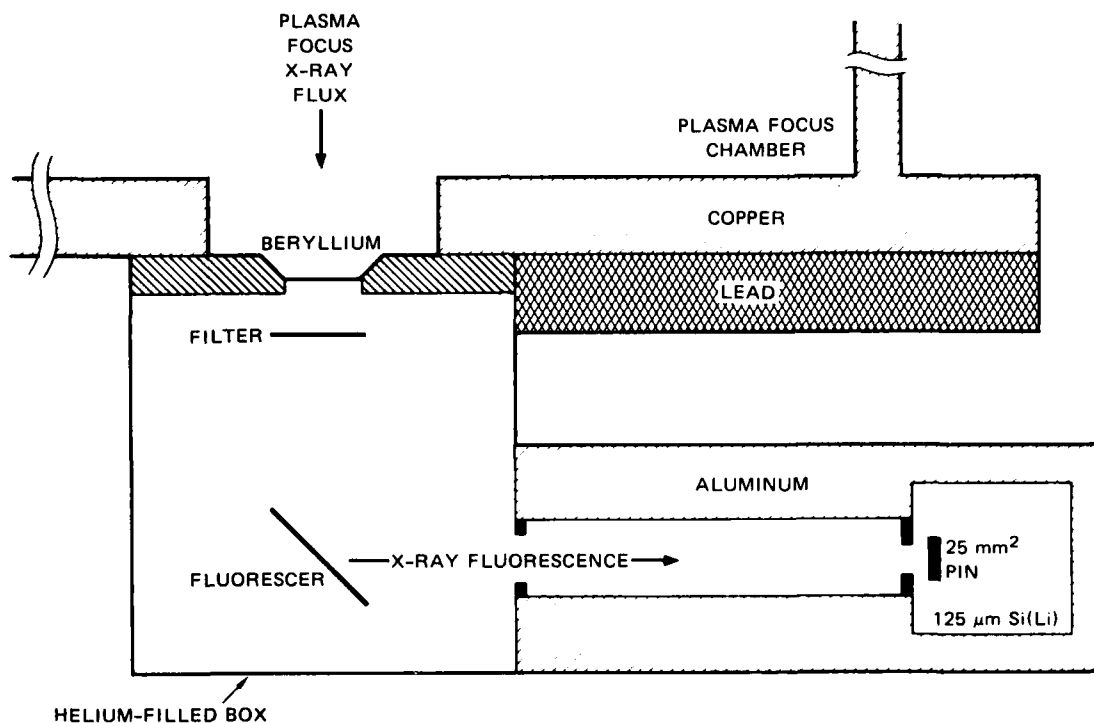


FIGURE 12 FILTERED-FLUORESCER-PIN X-RAY DETECTOR

bands were used in this geometry as in the fluorescer geometry. Figures 14(b), (c), and (d) are examples of the X-ray signals obtained using this geometry. Note that the very narrow portion of the X-ray pulse occurs in the 2.8- to 4.5-keV band, indicating intense line emission from argon, and note the occasional multiple occurrence of the spikes. In Figure 14(d), there are three spikes; although the middle one is clearly argon line radiation, the first and third ones (equal in intensity in both detectors) probably result from the beam hitting the pulse-gas tube, which was near the focus.

We obtained the following results with our X-ray measurements. The power, P , and energy, W , of the line emissions are about the same for plasma focus operation at 40 and 60 kV:

$$\begin{aligned} P_{\text{lines}} &\approx 0.4 \text{ GW} \\ W_{\text{lines}} &\approx 3 \text{ J} \end{aligned}$$

Out-of-band estimates for continuum radiation are:

$$\begin{aligned} W &\approx 0.5 - 1 \text{ J} & (40 \text{ kV operation}) \\ W &\approx 5 - 10 \text{ J} & (60 \text{ kV operation}). \end{aligned}$$

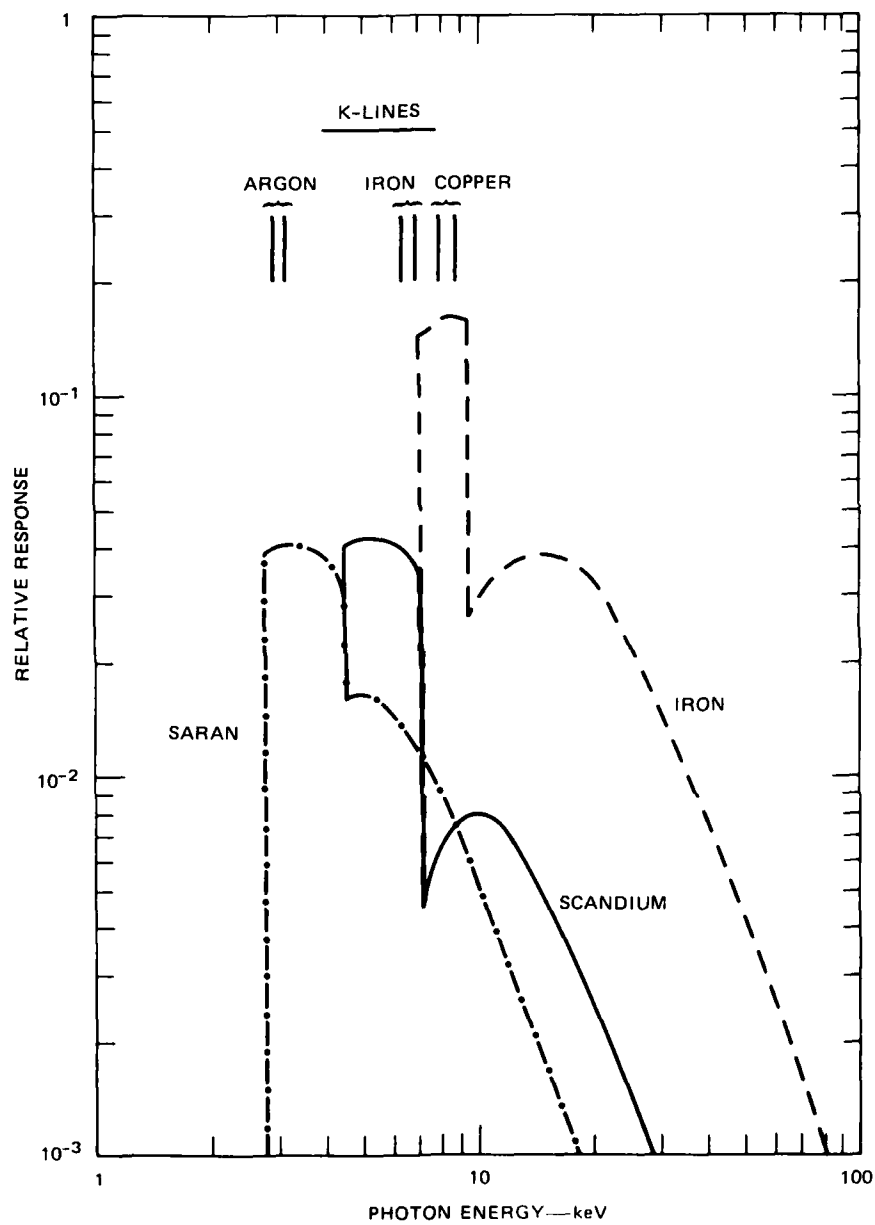


FIGURE 13 RESPONSE FUNCTIONS OF FILTER-FLUORESCER X-RAY DETECTORS

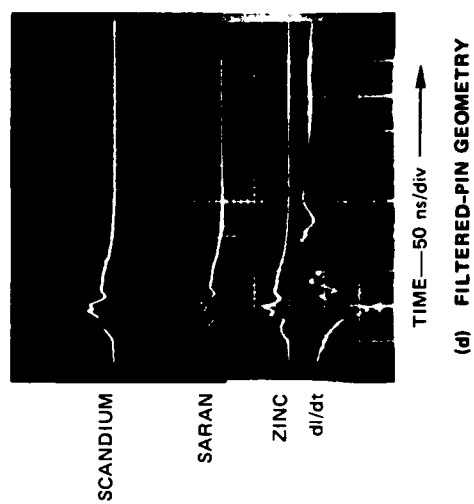
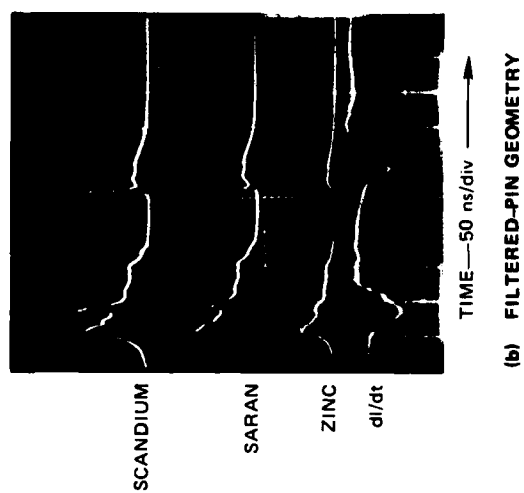
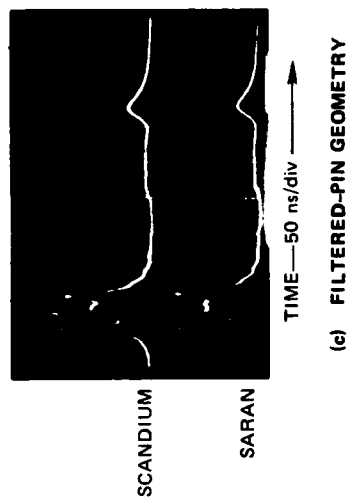
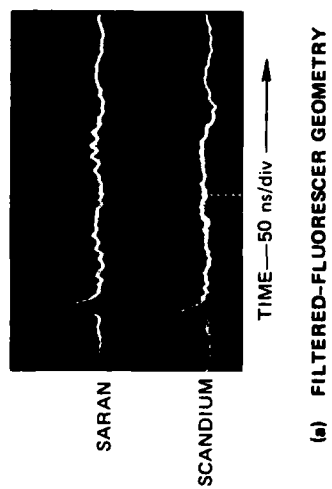


FIGURE 14 X-RAY SIGNALS FROM PIN DETECTORS IN FLUORESCER AND FILTERED-PIN GEOMETRIES

As noted before, we have not yet optimized the operation and X-ray output at 60 kV. However, our observations indicate that the intensity and energy in the very short pulse component of the radiation was about the same at 40 and 60 kV, but, the radiation in the longer-duration pulse increased by about a factor of ten when going from 40 to 60 kV. We also tend to see longer-lasting pulses at 60 kV.

C. Discussion of Results

We use two radiation models to interpret the X-ray measurements; these models are shown in Table 3. We presume the existence of plasma phenomena producing X rays and also the possible formation of a high-energy electron beam in the focus that could produce line radiation and bremsstrahlung. The equations for plasma radiation and the ratio of ion species are based on the steady-state corona model. In general, for the densities and temperatures that are expected in an argon plasma, the most intense radiation is from lines, and thereafter we find the recombination intensity and least of all, bremsstrahlung radiation. The bremsstrahlung and recombination spectra (dP/dE_v) are similar, as indicated in Table 3, except that the recombination spectra have a threshold at the ionization energy for the ions. Bremsstrahlung radiation dominates only when the plasma consists of primarily completely stripped ions. In argon, this occurs only for an electron temperature greater than about 13 keV.

Table 3

RADIATION MODELS FOR ARGON

(a) Plasma Model

$P_{\text{line}} \propto N_i^z N_e T_e^{-1/2} \exp(-E_{21}/T_e)$	
$P_{\text{recomb}} \propto E_z^2 N_i^{z+1} N_e T_e^{-1/2}$	$dP_r/dE_v \propto \exp \left[(E_z - E_v)/T_e \right]$
$P_{\text{brems}} \propto Z_i^z N_i^z N_e T_e^{1/2}$	$dP_b/dE_v \propto \exp \left[-E_v/T_e \right]$
$N_i^z/N_i^{z+1} \propto E_z^2 (E_z/T_e)^{3/4} \exp(E_z/T_e)$	

(b) Beam-Target Model for Argon

$P_{\text{line}} \approx 0.003 P_{\text{beam}}$	$P_{\text{beam}} = \bar{E} I$
$P_{\text{brems}} \approx 2.5 \times 10^{-9} \bar{E} P_{\text{beam}}$	

First we consider the very narrow (approximately 10 ns) X-ray pulses that consist primarily of the line radiation from argon or the gas tube material. In a beam model, high-energy electrons that collide with argon atoms and ions create K-shell vacancies with an efficiency independent of their kinetic energies, so long as that kinetic energy is much greater than the K-edge energy of argon. Using the expression for argon line intensity given in Table 3 and using the expression for beam power, our X-ray data show that the mean energy \bar{E} is greater than 100 keV. Entering this mean energy into the expression for bremsstrahlung power, we find that the expected bremsstrahlung from such a beam would be much less than the line intensity. This prediction is consistent with the observed X-ray measurements.

We do not believe that the plasma model can explain the very short pulse, which has most of its energy in the form of line radiation from argon (or from the inlet tube material). If the plasma were producing significant line radiation, it would necessarily also emit much recombination radiation, which would produce a large out-of-band signal; no such signal has been observed.

The long component of the X-ray pulse is difficult to explain using a beam model. The long component has little or no argon radiation present. To explain this with a beam model, we would need an unusually high mean electron energy, sufficient for the bremsstrahlung emission to dominate line emission. However, using the plasma model, we can determine two conditions. Since there is no in-band X-ray signal, the electron temperature is excluded from a range from 230 to 2900 eV. If the electron temperature is assumed to be less than 230 eV, it is difficult to explain the size of the observed signal. However, if the electron temperature is assumed to be greater than 2900 eV, we require a plasma diameter of about 1 cm to explain the observed intensity. If we assume a 1-mm diameter, the predicted intensity would be much much larger than seen. What is needed now is some pinhole X-ray photography to determine the actual radiating diameter of the plasma.

At this point, it is appropriate to comment on the scaling of the X-ray yield with increasing bank energy or current. Scaling up the yield by enhancing the beam-target X-ray emission in the focus is not a promising approach. (This could be done by increasing the mean electron energy or decreasing the pulse width. However, both of these quantities are already near what would be suitable for some purposes.) Therefore, the only feasible way to increase the X-ray output with the beam is to increase the power carried by the beam. We then expect the electron beam power to scale proportionally to the capacitor bank energy as one goes to large capacitor banks. This is not a favorable scaling law, considering the low efficiency of the electron beam for producing X-rays.

A much more favorable scaling relation is obtained when one considers the plasma radiation source. The X-ray yield scales roughly as I^4/r^2 , where r is the radius of the plasma focus. The focus radius is expected to decrease as the current is increased. Therefore, the scaling

could possibly go higher than the fourth power of the current. Thus, the X-ray yield from the plasma is expected to increase rapidly with increase of bank current until it becomes limited by the rate of power transfer to the plasma. At that point, the efficiency of radiation is much higher than for the beam target case and is a significant fraction of the total bank energy. Consequently, the prospects for this model favor going to higher bank voltages, for which higher currents are obtainable and higher energy transfer to the plasma is attainable for a given bank energy.

D. Radiation Model Prediction for Neon

This section describes a radiation model of the plasma focus that was developed to provide radiation emission predictions for various operating gases and gas mixtures. It is useful for operation at relatively high pressures, where the strong electron beam phenomena are not present.

The PF source produces most of its radiation in a small cylindrical volume (radius ≈ 1 mm, length ≈ 1 cm). The spectrum consists of a combination of discrete lines, recombination radiation, and bremsstrahlung continuum. The spectral location and relative importance of these components depend greatly on the gas species used, their relative concentrations, and the plasma temperature obtained in the source volume. For these reasons the PF source is capable of producing a wide range of spectral characteristics. We discuss here the plasma phenomena that power the radiation output and evaluate a potential method for greatly increasing the radiation production efficiency. This method requires operation with neon gas to produce a spectrum peak near 1 keV from intense line radiation.

The emission power density in a hydrogen-like plasma is given by (McWhirter, 1965):

$$P_{\text{line}} (\text{W/m}^3) = 5.05 \times 10^{-31} f_{12} N_{\text{ig}}^z N_e T_e^{-1/2} \exp(-E_{21}/T_e),$$

where

$E_{21} (\text{eV})$ = photon energy,

$N_{\text{ig}}^z (\text{m}^{-3})$ = ground-state density of ions with charge z ,

$N_e (\text{m}^{-3})$ = electron density,

$T (\text{eV})$ = electron temperature, and

f_{12} = absorption oscillator strength of the E_{21} transition.

To determine the parameters for this equation, we must first find the electron temperature that would produce a plasma containing predominantly hydrogen-like and helium-like ions. These ions are the most intense emitters of radiation. This may be done by examining the ratio of ion intensities as a function of temperature. The steady-state corona model is appropriate for the temperatures and densities of interest (McWhirter, 1965). It gives:

$$N_i^z/N_i^{z+1} = 7.87 \times 10^{-9} E_z^2 (E_z/T_e)^{3/4} \exp(E_z/T_e),$$

where

E_z (eV) = ionization potential of an ion specie in charge state z , and

$N_i^{z+1} (\text{m}^{-3})$ = density of an ion specie in charge state $z+1$.

The plasma density is needed to calculate the intensity of line emission. This is obtained by noting that at maximum compression, the magnetic pressure caused by the driving current is balanced by the plasma pressure. This expression for pressure balance is called the Bennett relation (Bennett, 1934):

$$\mu_0 I^2 / 8\pi = (n_e + n_i) kT (\pi r^2),$$

where

I = discharge current,

n_e and n_i = electron and ion densities, respectively,

T = plasma temperature, and

r = plasma radius.

The power radiated in lines can now be expressed in terms of the plasma current as follows:

$$P_{\text{line}} (\text{watts}) = 0.28 \times 10^{-12} I^4$$

for a new plasma focus with

$T_e = 0.28$ keV and

$r = 1$ mm.

Using the typical pulse width of 50 ns for this type of system (Gates, 1971) we find that the plasma energy is rapidly radiated away in the form of line radiation when the discharge current is large. A minimum capacitor bank size is about 2 kJ, above which the plasma density is high enough to radiate away most of the plasma energy during the pulse.

The pressure balance condition shows that 1 percent of the capacitor bank energy resides in plasma energy at maximum compression. We conservatively take this value of 1 percent to be the power conversion efficiency of the PF source. This estimate neglects the energy transferred from magnetic field to plasma during the radiation pulse and assumes only the internal energy in the plasma is radiated. Thus a 10-kJ capacitor bank transfers 100 J of energy into the compressed plasma, which is then radiated in the form of X-rays, provided that a suitable ion was chosen.

A computer solution of the equations described above has indicated that intense emission of radiation requires elements of lower atomic number than argon, because the plasma focus system that was used in this program was not capable of producing high percentages of hydrogen-like and helium-like argon ions. We describe here the predicted conditions for operation with neon gas in order to produce a 1 percent efficient emission of radiation from the plasma focus. This efficiency would be about 10 times that obtained with argon.

Although several elements are suitable candidates for an intense source, we chose to evaluate neon for this approach because it is an inert gas and has been used in a similar device in the past. We also operated our system with neon gas to insure that strong focusing occurred, but no radiation measurements were made because of the low photon energy. The spectral characteristics of neon are given in Table 4.

Table 4
SPECTRAL CHARACTERISTICS OF NEON

Lines		Lower Bound of Recombination Spectrum	
Charge State	$E_v(2p-1s)$ (keV)	Recombination Transition	$E_v(\min)$ (keV)
0	0.849	$10+ \rightarrow 9+$	1.362
7+	0.906	$9+ \rightarrow 8+$	1.196
8+	0.922	$8+ \rightarrow 7+$	0.239
9+	1.022	$7+ \rightarrow 6+$	0.207

Ne^{9+} and Ne^{8+} are hydrogen-like and helium-like ions that have principal resonance lines at 1.21 and 1.35 nm on the $n = 2$ to $n = 1$ transition. Using $E_9 = 1362$ eV, $E_8 = 1196$ eV, and $E_7 = 239$ eV, we find that the plasma temperature range for which the density of Ne^{8+} or Ne^{9+} ions exceeds that of Ne^{7+} and Ne^{10+} is $38 < T_e < 410$ eV. The temperature for which there would be equal densities of Ne^{8+} and Ne^{9+} is $T_e \approx 340$ eV; these ions would then constitute about 82 percent of the Ne ions.

To obtain more accurate values of the optimum plasma temperature and radiation yield, we used published values of the line intensities for helium-like, hydrogen-like, and lithium-like ions of neon (Wiese, 1966; Kelly, 1973). We found that the maximum line emission occurs at a temperature of about 0.28 keV, as shown in Figure 15. Comparing the line intensity with the intensity of recombination and bremsstrahlung continuum reveals that these emissions amount to about 17 percent of the power radiated in lines near 1 keV.

In summary, we have assumed a 50-ns radiation pulse from a source volume 1-cm long by 1-mm radius and an electron temperature of 280 eV. These parameters produce neon ions in charge states 7, 8, 9, and 10 with fractional densities of 0.0006, 0.67, 0.28, and 0.045, respectively. A 10-kJ capacitor bank that provides a pinch current of 450 kA would produce a total radiated energy of 100 J in lines near 1 keV. Additionally, about 17 J would be emitted as recombination and bremsstrahlung, which has a peak intensity per unit wavelength interval at 680 eV and about 95 percent of its spectral energy content below 2 keV.

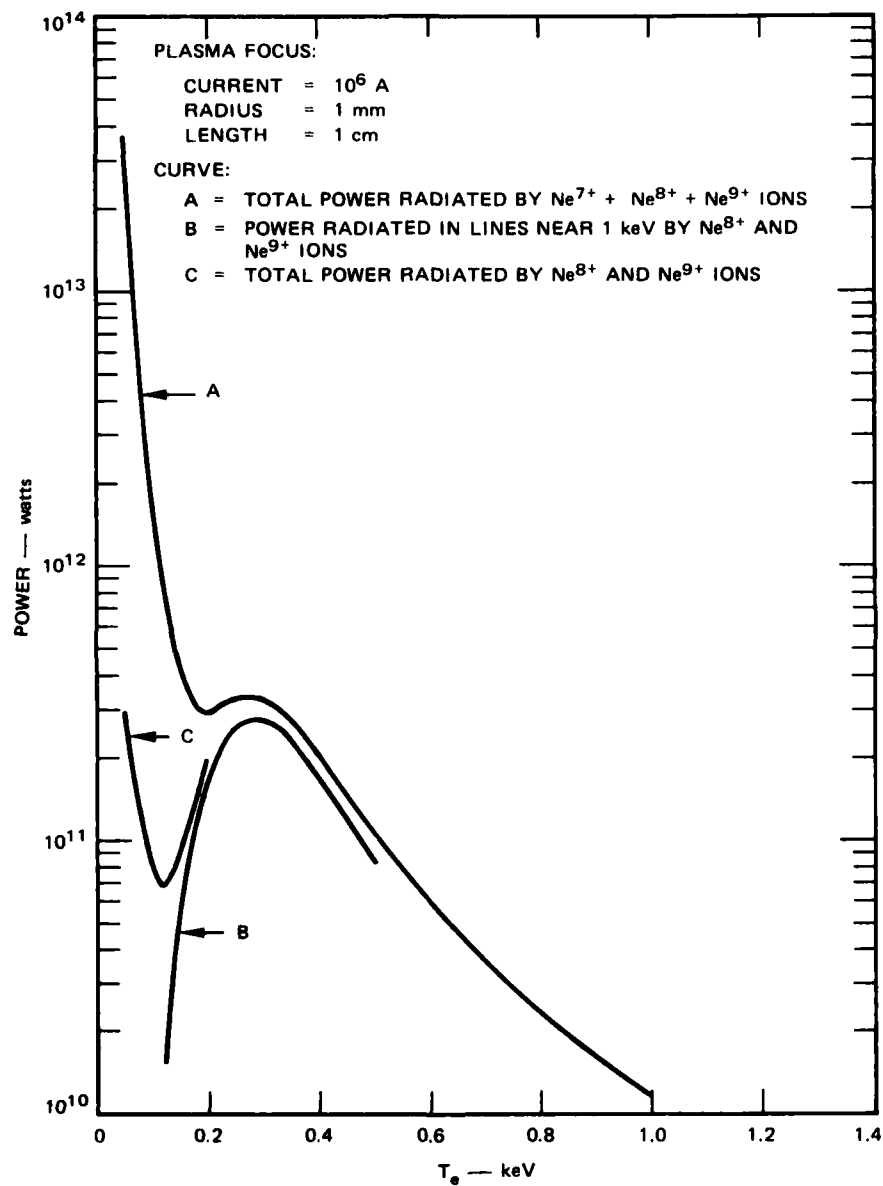


FIGURE 15 POWER RADIATED BY NEON PLASMA

V 120-kV PLASMA FOCUS SYSTEM

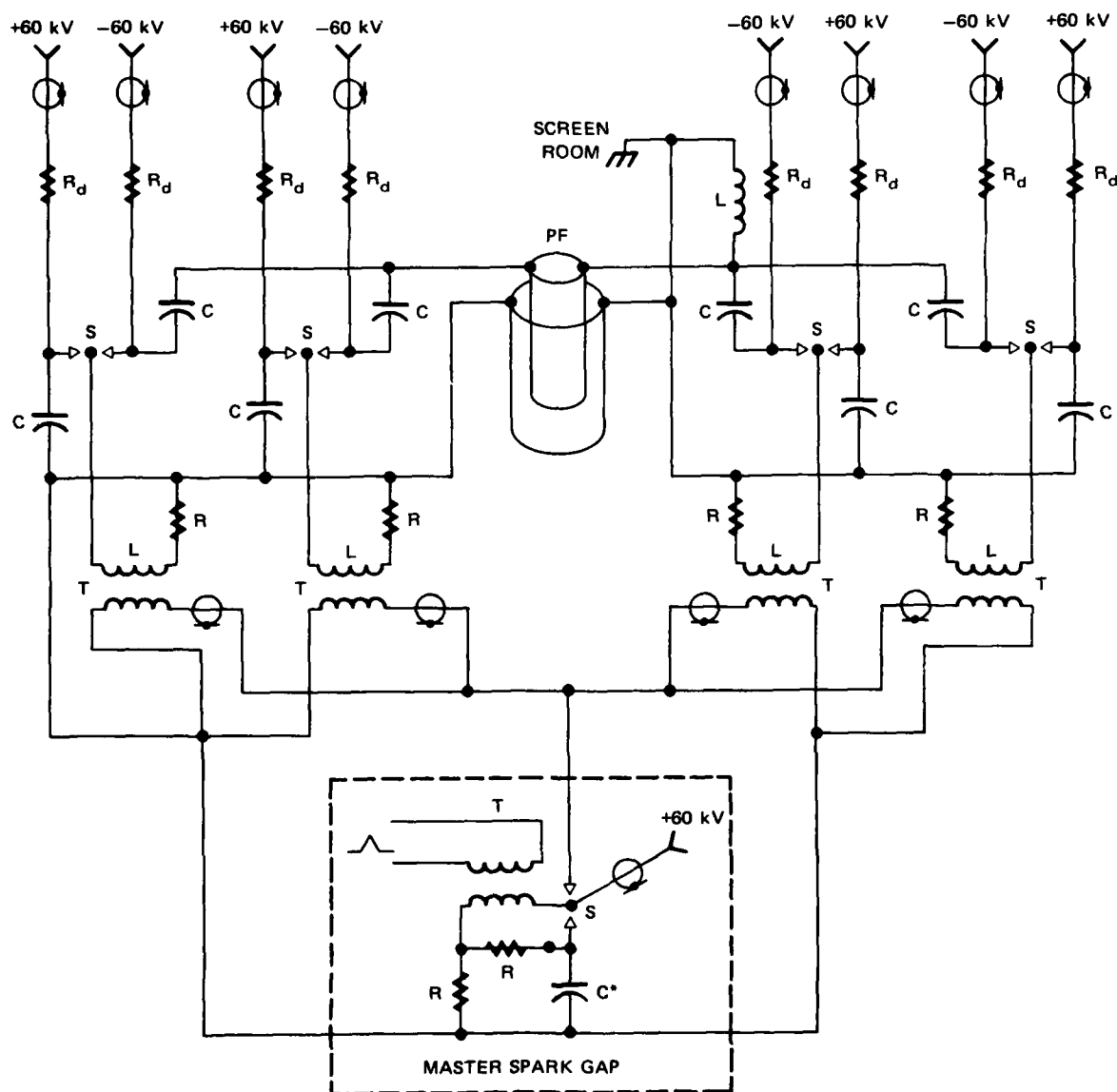
At the end of this program a 120-kV, 108-kJ plasma focus system was built to expand the range of the high voltage study. The new PF system was designed to drive the same load that was used on the 60-kV system. The new system also used the same type of 60-kV capacitors and pressurized spark-gap switches that were used in the 60-kV system. However, the design of the capacitor bank was significantly different. A +/- charging system was utilized, because 120-kV capacitors were not available.

A schematic diagram of the capacitor bank charging arrangement is shown in Figure 16. Groups of four capacitors are arranged in series with a pressurized spark gap switch to hold off the voltage during charging. One group of capacitors is charged to a negative voltage, and the other group is charged to a positive voltage. Thus the voltage across the switch is twice the charging voltage, which is also the voltage that appears at the plasma focus load when the switches are triggered.

The other major design change from the lower voltage system was that the capacitors were immersed in oil to insulate against the higher voltages and to provide an overall smaller package for the system. A great savings in system inductance was also made by connecting the capacitors to the load with parallel plate transmission lines rather than with the coaxial cables used in the other system. The capacitor bank was divided into two major units, each of which was placed in a steel tank for oil immersion. A cutaway drawing of one of these tanks is shown in Figure 17. The PF load (Figure 4) was installed between the two tanks.

The 120-kV PF system has a capacitance of 15 μF and a predicted inductance of about 30 nH. Because of its lower inductance, it should produce about 20 percent larger peak current than the 60-kV system; i.e., about 1.8 MA into the PF load.

Unfortunately, the system was not operated because of a technical difficulty that occurred when the insulating oil was transferred into the tanks. It takes ten 55-gallon drums to fill the system: One of the drums of oil used to fill the system was contaminated with water, probably as a result of being stored outside for a number of months. This water caused the capacitor bank to short out to ground during high-voltage tests. As a result, it appears that the standoff insulators in the bottom of one of the tanks were damaged, as it will no longer hold high voltage. It will be necessary to repair this insulation before the system can be operated, but it might be possible to disconnect the inoperative tank and operate the PF system at one-half energy using only the operative half of the capacitor bank.



$C = 7.5 \mu F$ (FOUR 60 kV CAPACITORS)
 S = PRESSURIZED SPARK GAP SWITCH
 $R_d = 5 k\Omega$ DUMP RESISTOR ($Cu SO_4$ SOLUTION)

T = TRIGGER TRANSFORMER
 C^* = ONE 60 kV CAPACITOR

FIGURE 16 CAPACITOR BANK AND MASTER SWITCH CIRCUITS FOR 120-kV PLASMA FOCUS SYSTEM

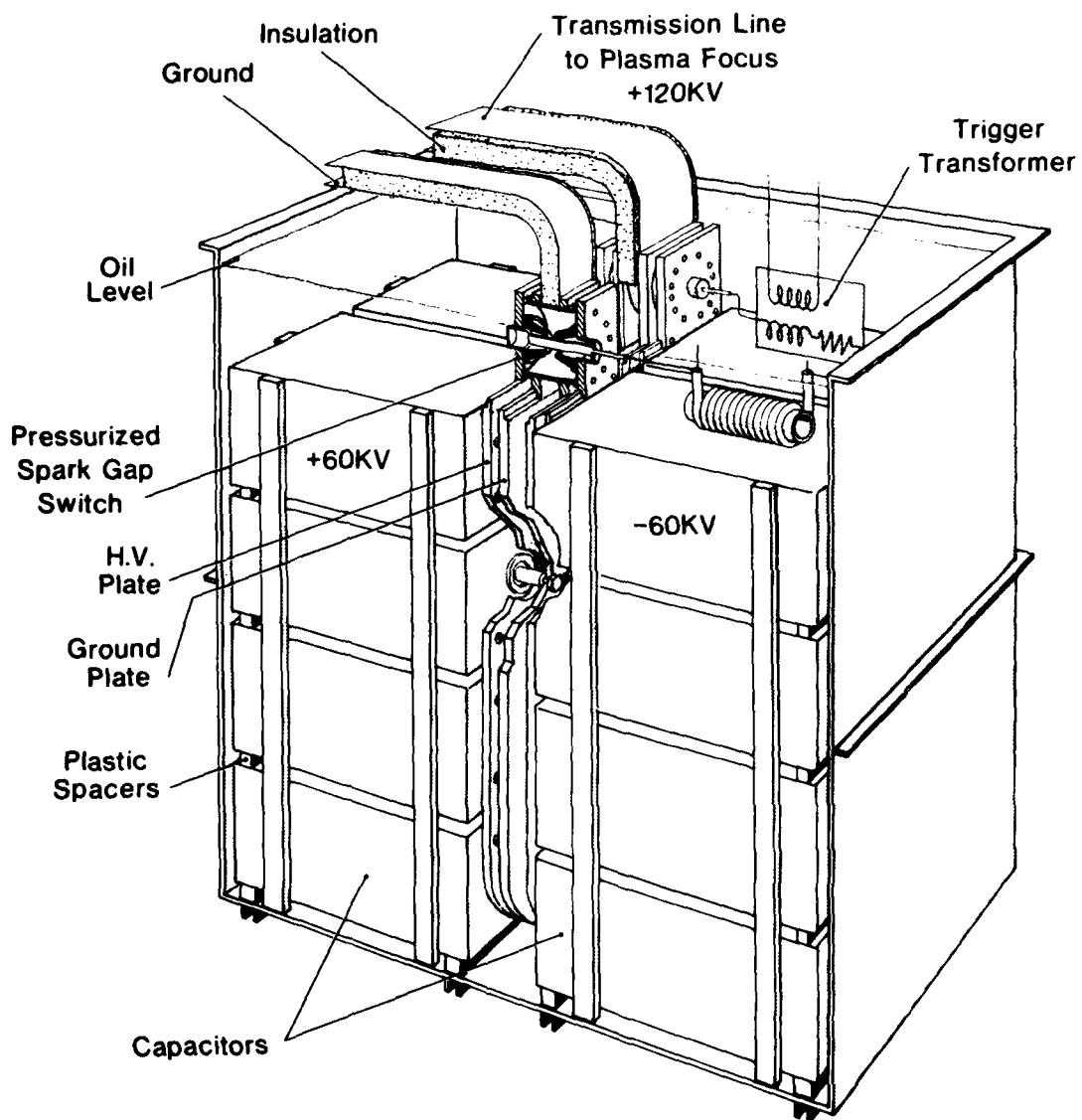


FIGURE 17 120-kV, 54-kJ SECTION OF CAPACITOR BANK FOR A PLASMA FOCUS DEVICE

VI RECOMMENDATIONS FOR FURTHER RESEARCH

Among the possible future directions for plasma focus research, we believe that the following three are of high priority:

- Cylinders
- Higher voltage
- High-Z ions.

We had planned to introduce thin-wall foil cylinders into the 120-kV plasma focus system. A photograph of one of these cylinders is shown in Figure 18. The cylinders are about 60 mils in diameter and have a wall thickness of 1 to 2 μm . The material is copper. The cylinders would have been used to study the effects of e-beam bombardment and to evaluate the possibility of getting a separation between the gas specie inside the cylinder and a different specie outside. Gribkov (at the Lebedev Institute in Moscow) observed heating of the target with a focus-produced electron beam. (Gribkov, 1978) He also believes that he has observed anomalous energy absorption in the plasma. This phenomenon bears further investigation.

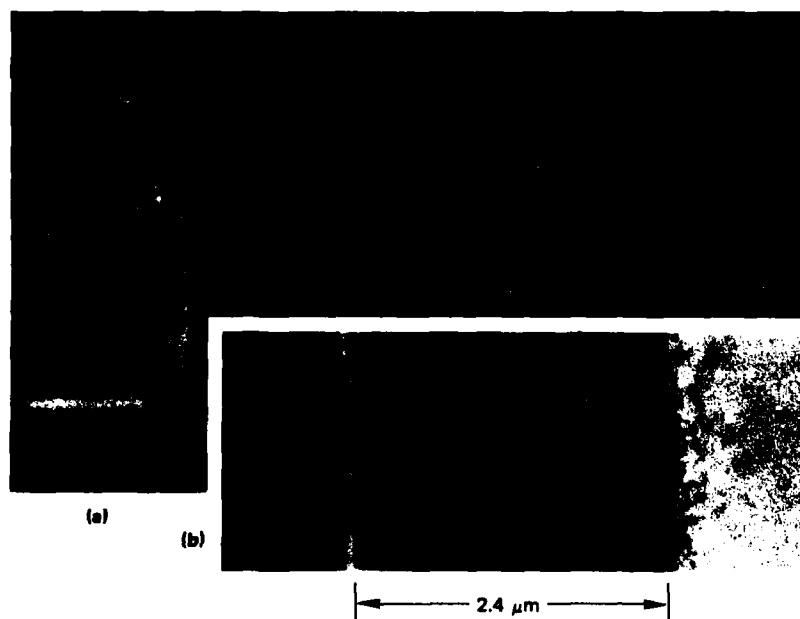


FIGURE 18 THIN-WALL CU CYLINDER (a) AND
MAGNIFIED WALL CROSS SECTION (b)

Although the e-beam is not very efficient in directly producing radiation, the efficiency could be greatly enhanced if the e-beam energy were deposited into the plasma, thereby heating it and producing more radiation from the plasma. The Darmstadt plasma focus group recently recorded the occurrence of possible lasing in the plasma as a result of the electron beam pulse (Herziger, 1978). This phenomenon should also be investigated further.

Higher-voltage plasma focus operation--100 to 120 kV--should be investigated to improve the peak current and power transferred to the plasma focus during the pinch phase. The new capacitor bank, described in Section V, could be used for these studies.

Bostick and Nardi (Bostick, 1977), Gullickson (Gullickson, 1978), and others reported the observation of high-energy deuterium ions produced by the plasma focus. It seems reasonable that high-energy ions of higher atomic numbers could be produced by the high electric field present in the focus. Since the focus is capable of stripping ions to very high levels, it is quite possible to produce MeV ions of high atomic numbers. These might be useful for collisional and charge exchange studies or for inertial confinement fusion.

VII LIST OF PUBLICATIONS RESULTING FROM THIS PROJECT

1. Gates, D.C., 1977: "X-Ray Emission from Plasma Focus in Puffed Gas," IEEE 1977 Int. Conf. on Plasma Sci., Catalog No. 77CH1205-4 NPS, p. 221 (IEEE, New York, New York).
2. Gates, D.C., 1978: "Electrodynamics and X-Ray Emission of a 60 kV Plasma Focus," IEEE 1978 Int. Conf. on Plasma Sci., Catalog No. 78CH1357-3 NPS (IEEE, New York, New York) p. 329.
3. Gates, D.C., 1978: "Studies of a 60 kV Plasma Focus," Second International Conference on Energy Storage, Compression and Switching, Venice, Italy (December); to be published.

REFERENCES

- Bennett, W.H., 1934: "Magnetically Self-Focussing Streams," Phys. Rev. 45, pp. 890-897.
- Bernstein, M.J., D.A. Meskan, and H.L.L. van Paassen, 1969: "Space, Time, and Energy Distribution of Neutrons and X-Rays from a Focused Plasma Discharge," Phys. Fluids, Vol. 12, No. 10, p. 2193.
- Bostick, W.H., V. Nardi, W. Prior, 1977: "Ion Beams from Focused Discharges: Energy Spectrum," Bull. Am. Phys. Soc., Vol. 22, No. 9, 1212. Abstract 10C11.
- Brown, S.C. 1959: Basic Data of Plasma Physics (John Wiley & Sons, New York). See especially Figures 4.51b and 14.10.
- Bruzzzone et al. 1976: Nuclear Fusion, Vol. 16, No. 5, pp. 870-873.
- Decker, G. and R. Wienecke, 1976: "Plasma Focus Devices," Physica, Vol. 8C, pp. 155-164 (March-April).
- Decker, G., L. Flemming, H.J. Kaeppler, T. Openländer, G. Pross, P. Schilling, H. Schmidt, and M. Trunk, 1977: "Current and Neutron Yield Scaling of Fast High Voltage Plasma Focus," Report IPF-77-2, Institut für Plasmaforschung, Stuttgart.
- Downing, J.N., D.A. Freiwald and J.W. Mather, 1973: "Performance Survey of a 212 kJ Dense Plasma Focus," Bull. Am. Phys. Soc. II, 18(10), p. 1363.
- Gates, D.C., L. Demeter, and A. Noeth, 1971: "Final Development of Coaxial Plasma Gun," Contract F2901-69-C-0103, Project AF-133B, Technical Report AFWL TR-70-159, Order No. AD-516 609L, Physics International, San Leandro, California (June) SECRET.
- Gates, D.C., 1977: "X-Ray Emission from Plasma Focus in Puffed Gas," IEEE 1977 Int. Conf. on Plasma Sci., Catalog No. 77CH1205-4 NPS, p. 221 (IEEE, New York, New York).
- Gates, D.C., 1978a: "Electrodynamics and X-Ray Emission of a 60-kV Plasma Focus," IEEE 1978 Int. Conf. on Plasma Sci., Catalog No. 78CH1357-3 NPS (IEEE, New York, New York) p. 329.
- Gates, D.C., 1978b: "Studies of a 60-kV Plasma Focus," Second International Conference on Energy Storage, Compression and Switching, Venice, Italy (December); to be published.

- Gribkov, V.A., 1978: "The FLORA Installation. Capabilities and Specifics of the Use of High-Current Relativistic Electron Flux Sources Based on the Z-Pinch to Heat a Plasma," UCRL-Trans-11214 (June).
- Gullickson, R.L. and H.L. Sahlin, 1978: "Measurements of High-Energy Deuterons in the Plasma-Focus Device," J. Appl. Phys., Vol. 49, No. 3, pp. 1099-1105.
- Herziger, G. et al., 1978: "Collimated Soft X-Rays from the Plasma Focus," Physics Letters, Vol. 64A, No. 4, pp. 390-392.
- Imshennik, V.S., N.V. Filippov, and T.I. Filippova, 1973: "Similarity Theory and Increased Neutron Yield in a Plasma Focus," Nucl. Fusion, Vol. 13, pp. 929-934.
- Kaeppler, H.J., 1977: "Basic Physical Phenomena, Neutron Production and Scaling of the Dense Plasma Focus," Report IPF-77-7, Institut für Plasmaforschung, Stuttgart.
- Kelly, R.L., and L.J. Palumbo, 1973: Atomic and Ionic Emission Lines Below 2000 Angstroms--Hydrogen through Krypton, NRL Report 7599 (Supt. of Documents, U.S. Govt. Printing Office, Washington, D.C. 20402).
- McWhirter, R.W.P., 1965: "Spectral Intensities," in Plasma Diagnostic Techniques, Edited by R.H. Huddleston and S.L. Leonard, pp. 201-264 (Academic Press, New York, New York).
- Mather, J.W., 1964: "Investigation of the High-Energy Acceleration Mode in the Coaxial Gun," Phys. Fluids (Suppl.) Vol. 7, No. 11, p. 528.
- Mather, J.W., 1971a: "Dense Plasma Focus," in Methods of Experimental Physics, Vol. 9B, pp. 187-249 (Academic Press, New York, New York).
- Mather, J.W., 1971b: 4th Conf. on Plasma Physics and Nuclear Fusion, Wisconsin.
- Trunk, M., 1975: "Numerical Parameter Studies for the Dense Plasma Focus," Plasma Physics, Vol. 17, pp. 237-248.
- Ware, K.D., A.H. Williams and R.W. Clark, 1973: "Operation of a 720 kJ, 60 kV Dense Plasma Focus," Bull. Am. Phys. Soc. II, Vol. 18(10), p. 1364.
- Wiese, W.L., M.W. Smith, and B.M. Glennon, 1966: Atomic Transition Probabilities: Vol. I, Hydrogen Through Neon, NSRDS-NBS4 (Supt. of Documents, U.S. Govt. Printing Office, Washington, D.C. 20402).